SUPPLEMENTAL MATERIAL

MONTE CARLO SIMULATION FOR DM-REFLECTION INSIDE THE SUN

In this section, we provide details on the Monte Carlo program that simulates the reflection of the DM particles from solar electrons. Our program derives both the spectrum of reflected DM and the magnitude of the reflected flux. The simulated flux is then used to derive the expected signal in dark matter detectors along the procedure described in the main text with additional details provided in the subsequent sections.

Our starting point is the standard Maxwell-Boltzmann velocity distribution for galactic DM as it standardly used in direct detection analyses. Irrespective of the details of the assumed galactic velocity distribution, once DM reaches the sun, its velocity will become dominated by the sun's gravity. One of the variables in the simulation is the impact parameter ρ of an incoming DM particle. In the absence of gravitational focussing the relevant range of ρ is limited from above by the solar radius $R_\odot$. The simulation scans the range of impact parameters $0 \leq \rho \leq 4R_\odot$; larger impact parameters do not change the result as the majority of DM particles in that case misses the Sun. We have numerically checked that the resulting magnitude of the reflected flux and the energy spectrum of the DM coming leaving the Sun do not change if we change the range of the impact parameter from $4R_\odot$ to $3R_\odot$. The initial conditions of each DM particle are generated by randomly sampling the velocity from the Maxwell-Boltzmann distribution and by choosing the impact parameter evenly from a disc with the radius of $4R_\odot$.

When a DM particle is outside the Sun, we calculate its trajectory analytically following Newton's law. Using the classical trajectory we determine the incident angle and velocity at the surface of the Sun. Once the DM particle is inside the Sun, for a given cross section, we calculate the mean free path $l_{\rm fp}(r)$ of the DM particle at each radial location r inside the Sun,

$$l_{\rm fp}(r) = [\sigma_e n_e(r)]^{-1} \ . \tag{S1}$$

The input used for this calculation (the electron density inside the Sun n_e) is obtained from the standard solar model of Bahcall [S1], with competing solar models such as [S2] yielding identical results (see Fig. S1). We then compare $0.1 \times l_{\rm fp}$ with $l_0 \equiv 0.01 \times R_\odot$, and choose the smaller to be the step size ($l_{\rm step}$) for tracing the trajectory inside the Sun. The probability of DM particle to scatter with an electron within one step is

$$P_c = 1 - e^{-l_{\rm step}/l_{\rm fp}} \ . \tag{S2}$$

Then we generate a number ξ with a flat random distribution from 0 to 1. If $\xi < P_c$, there is no scattering and we move the DM particle to the end point of this step while changing its velocity according to the gravitational potential.

If $\xi > P_c$ the DM particle scatters with an electron within this step. We randomly generate the initial energy and momentum of the electron according to the local temperature of the Sun. Then we boost the DM particle and the electron to their center-of-mass frame. Then following the differential cross section we randomly generate the directions of the outgoing DM particle and the electron. Then we boost them back to the solar frame. (The interactions considered in this paper are contact-type, as the mass of the mediator particle is assumed to be larger than maximum momentum transfer. This simplifies the distribution of the final state momenta in the collision.)

At each step we monitor if the DM particle leaves the Sun. Once it is out of the Sun, we calculate its kinetic energy plus the potential energy from the solar gravity and then put it into a histogram. Since the initial impact parameter is from 0 to $4R_\odot$, there is a chance that the DM particle never passes through the Sun. If this happens we put the initial kinetic energy of this particle into the histogram. Then we normalize the histogram to get a normalized distribution of the energy spectrum of solar reflected DM, which is $F_{A_\rho}(E)$ above Eq. (3) in the paper.

The normalized histograms for $m_{\rm DM} = 3$ MeV for different cross sections are shown in Fig. 3 in the paper. For larger values of σ_e, the DM particle prefers to collide with the electrons in the outer layers of the Sun, and therefore the energy it acquires from the Sun is relatively smaller due to lower temperatures. Whereas in the case of smaller cross sections, the DM particle can penetrate deeper and acquire larger energy through collisions with hotter electrons. This explains why the red curve in the Fig. 3 drops earlier compared to the rest.

A brief summary of the main features of the reflected flux of the DM particles is shown in Tab. I. For each value of the dark matter mass and scattering cross section the average energy of the reflected DM, the endpoint of the reflected DM spectrum (defined as the upper limit of the energy interval containing 95% of the reflected flux), and the total value of the reflected DM flux at the earth position are shown. The endpoint energy in the reflected spectrum should be compared with the galactic endpoint, $m_{\rm DM} v_{\rm esc}^2/2$, where $v_{\rm esc}$ is the escape velocity, quantifying the hardening of the reflected spectrum. This ratio is found to be in the range 100–7000 for the parameters listed in the table.

	10^{-38} cm^2	10^{-37} cm^2	10^{-36} cm^2	10^{-35} cm^2	10^{-34} cm^2
0.1 MeV	289 eV	294 eV	335 eV	395 eV	286 eV
	989 eV	1011 eV	1169 eV	1471 eV	1024 eV
	4.2 cm^{-2}sec^{-1}	40 cm^{-2}sec^{-1}	318 cm^{-2}sec^{-1}	1150 cm^{-2}sec^{-1}	2302 cm^{-2}sec^{-1}
0.2 MeV	419 eV	427 eV	465 eV	478 eV	328 eV
	1431 eV	1460 eV	1604 eV	1657 eV	1094 eV
	2.1 cm^{-2}sec^{-1}	20 cm^{-2}sec^{-1}	159 cm^{-2}sec^{-1}	576 cm^{-2}sec^{-1}	1156 cm^{-2}sec^{-1}
0.5 MeV	516 eV	518 eV	552 eV	532 eV	355 eV
	1773 eV	1774 eV	1874 eV	1774 eV	1142 eV
	0.81 cm^{-2}sec^{-1}	8.0 cm^{-2}sec^{-1}	63 cm^{-2}sec^{-1}	229 cm^{-2}sec^{-1}	458 cm^{-2}sec^{-1}
2 MeV	356 eV	359 eV	400 eV	452 eV	331 eV
	1205 eV	1218 eV	1375 eV	1607 eV	1125 eV
	0.2 cm^{-2}sec^{-1}	1.9 cm^{-2}sec^{-1}	15 cm^{-2}sec^{-1}	56 cm^{-2}sec^{-1}	112 cm^{-2}sec^{-1}
4 MeV	245 eV	224 eV	283 eV	382 eV	318 eV
	799 eV	804 eV	959 eV	1428 eV	1141 eV
	0.09 cm^{-2}sec^{-1}	0.88 cm^{-2}sec^{-1}	7.1 cm^{-2}sec^{-1}	26 cm^{-2}sec^{-1}	52 cm^{-2}sec^{-1}

TABLE I. Features of the reflected DM flux on the earth. For each value of the DM mass the first and second row show the average energy and the end point energy of the reflected DM flux; the third row is the flux of DM at the surface of the earth.

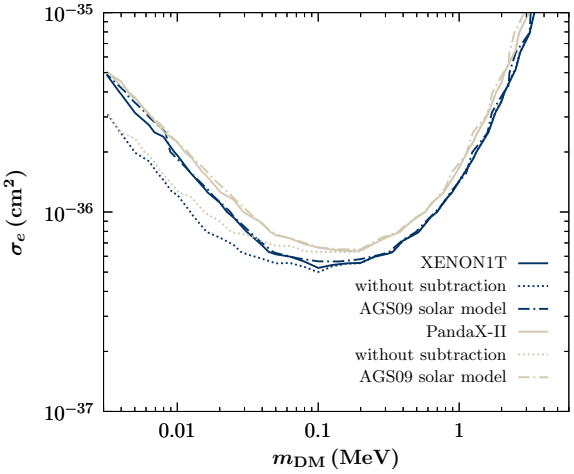

FIG. S1. Impact of various systematic theoretical uncertainties on the direct detection limits originating from the solar reflection process as well as from the evaluation of the atomic scattering cross section.

EVALUATION OF THE DM ELECTRON SCATTERING CROSS SECTION

Here we provide the details of our evaluation of the DM(χ)-electron(e) scattering cross section. We treat the electron recoil nonrelativistically, $E'_e = m_e + E_{R,e}$ with $E_{R,e} \ll m_e$, but allow for the general case when the incoming DM particle may be relativistic. From the definition of momentum transfer $\vec{q} = \vec{p}_\chi - \vec{p}'_\chi$, energy conservation gives the total amount of energy lost by DM in the collision and hence deposited in the detector,

$$E_{\rm dep.} = E_\chi - E'_\chi = m_\chi \left[\sqrt{1 + \frac{\vec{p}_\chi^{\,2}}{m_\chi^2}} - \sqrt{1 + \frac{|\vec{p}_\chi - \vec{q}|^2}{m_\chi^2}} \right]. \tag{S3}$$

The scattering cross section on bound electrons is conveniently normalized to the non-relativistic cross section σ_e on a free electron (see, *e.g.* [S3]), $\sigma_e \equiv \mu_{{\rm DM},e}^2 \overline{|M(q = \alpha m_e, E_\chi \to m_\chi)|}^2 / (16\pi m_{\rm DM}^2 m_e^2)$, where the square of scattering amplitude is summed (averaged) over intial (final) state spins. The latter is evaluated at a momentum transfer characteristic for an atomic process, $q = |\vec{q}| = \alpha m_e$, with any remaining q-dependence and/or χ-energy dependence absorbed by a DM form factor $F_{\rm DM}$, $\overline{|M(q, E_\chi)|}^2 = \overline{|M(q = \alpha m_e, E_\chi \to m_\chi)|}^2 \times |F_{\rm DM}(q, E_\chi)|^2$. For the purpose of

this paper, we consider the simple case of a contact interaction for which $F_{DM} = 1$ while more general cases are obtained in a straightforward manner.

The differential electron recoil rate resulting from ionization of atomic state with principal and angular quantum numbers n and l can be brought into the form,

$$\frac{d\sigma_{nl}v}{d\ln E_{R,e}} = \frac{\sigma_e}{16\pi}\frac{m_\chi^2}{\mu_{\chi e}^2}\int d\Omega_{\vec{p}'_e}\frac{d^3\vec{q}}{E_\chi E'_\chi}\,|F_{\rm DM}(q,E_\chi)|^2|f_{nl}(q)|^2\delta(E_{\rm dep.}-\Delta E_e) \tag{S4}$$

where $\Delta E_e = E_{R,e} + |E_B|$. The δ-function can be used to perform the angular part of the integral in $d^3\vec{q}$,

$$\frac{d\sigma_{nl}v}{d\ln E_{R,e}} = \frac{\bar{\sigma}_e}{8\mu_{\chi e}^2}\frac{m_\chi^2}{p_\chi E_\chi}\int dq d\Omega_{\vec{p}'_e}\,q|f_{nl}(q)|^2|F_{\rm DM}(q,E_\chi)|^2. \tag{S5}$$

A factor $1/v$ in the usual expression of galactic DM-electron scattering is being replaced by the more general factor $m_\chi^2/(p_\chi E_\chi)$. The ionization form factor is given by,

$$|f_{nl}(q,p'_e)|^2 = \frac{p'_e}{\pi^2 q}\int_{|p'_e-q|}^{p'_e+q}dp'\,p'\sum_{m=-l}^{l}|\langle\vec{p}'_e|e^{i\vec{q}\cdot\vec{r}}|nlm\rangle|^2, \tag{S6}$$

where $\vec{p}' \equiv \vec{p}'_e - \vec{q}$. For very light DM, $|\vec{q}\cdot\vec{r}| \ll 1$ may be attained in the evaluation of (S6). If the final state wave function is approximated by a plane or Coulomb wave, and not the exact atomic electron wave function, the bound and scattering states are not guaranteed to be orthogonal, $\langle nlm|\vec{p}'_e\rangle \neq 0$. To avoid spurious contributions in the approximations employed we modify the transition matrix element by subtracting the unity operator,

$$\langle\vec{p}'_e|e^{i\vec{q}\cdot\vec{r}}|nlm\rangle \to \langle\vec{p}'_e|e^{i\vec{q}\cdot\vec{r}}-1|nlm\rangle = \chi_{nl}(p')Y_{lm}(\hat{p}') - \chi_{nl}(p'_e)Y_{lm}(\hat{p}'_e) \tag{S7}$$

where χ_{nl} is the fourier transform of the radial Hartree-Fock wave function R_{nl}, $\chi_{nl}(q) = 4\pi(-1)^l i^l\int dr\,r^2R_{nl}(r)j_l(qr)$. Explicitly, one finds,

$$\begin{aligned}\int d\Omega_{\vec{p}'_e}\sum_{m=-l}^{l}|\langle\vec{p}'_e|e^{i\vec{q}\cdot\vec{r}}-1|nlm\rangle|^2 &= \frac{2l+1}{2p'_e q}\int_{|p'_e-q|}^{p'_e+q}dp'\;p'|\chi_{nl}(p')|^2\\ &+ (2l+1)|\chi_{nl}(p'_e)|^2 - (-1)^l\frac{2l+1}{2\pi}\chi_{nl}(p'_e)\int d\Omega_{\vec{p}'_e}\;\chi_{nl}(p')P_l(\hat{p}'\cdot\hat{p}'_e).\end{aligned} \tag{S8}$$

The first term on the right hand side is the DM-electron scattering form factor previously obtained in the literature [S3] while the subsequent terms originate from the subtraction. The remaining angular integral is evaluated as,

$$\int d\Omega_{\vec{p}'_e}\;\chi_{nl}(p')P_l(\hat{p}'\cdot\hat{p}'_e) = 2\pi\int_{-1}^{+1}d\cos\theta\;\chi_{nl}\left(\sqrt{p'^2_e+q^2-2p'_e q\cos\theta}\right)P_l\left(\frac{p'_e-q\cos\theta}{\sqrt{p'^2_e+q^2-2p'_e q\cos\theta}}\right). \tag{S9}$$

Since two unit vectors are dotted as argument of the Legendre polynomial P_l, the latter integrand is always well-behaved. One can verify that the subtraction works by noting that,

$$\frac{2l+1}{2p'_e q}\int_{|p'_e-q|}^{p'_e+q}dp'\;p'|\chi_{nl}(p')|^2 \to (2l+1)|\chi_{nl}(p'_e)|^2 \qquad (q\to 0), \tag{S10}$$

and that $P_l(1) = 1$ so that Eq. (S8) indeed vanishes identically for $q \to 0$. We have also verified this numerically in our computer code. It turns out that the subtraction has only a relatively minor influence on the derived bounds, see Fig. S1. We note in passing that the case considered here is quite different from the case when DM is slow and $|\vec{q}\cdot\vec{r}| \gg 1$ for which the ionization process becomes short-distance dominated, and a relativistic atomic treatment becomes necessary [S4].

The minimum incoming momentum to produce an electron recoil $E_{R,e}$ is obtained from the δ-function in (S4) when $\vec{q}$ and $\vec{p}_\chi$ are parallel, *i.e.* $\cos\theta_{qp_\chi} = 1$,

$$p_\chi^{\rm min} = \frac{q}{2(1-\Delta E_e^2/q^2)}\left[1-\frac{\Delta E_e^2}{q^2}+\frac{\Delta E_e}{q}\sqrt{\left(1-\frac{\Delta E_e^2}{q^2}\right)\left(1+\frac{4m_\chi^2}{q^2}-\frac{\Delta E_e^2}{q^2}\right)}\right]. \tag{S11}$$

This expression is exact and is used in the integral that computes the average over the incoming energy spectrum (see main text). In the non-relativistic limit, expanding in $\Delta E_e/q \ll 1$ one recovers the expression for $v_{\rm min} = p_\chi^{\rm min}/m_\chi$ given in previous works [S3].

MODELING OF LXE DETECTOR RESPONSE

Here we describe a simple procedure that is aimed at capturing the dominating factors in the detection of scintillation (S1) and ionization (S2) signals following an electron recoil in a LXE detector. Our treatment largely follows previous experimental, theoretical, and joint theory-experiment studies [S5–S7]. With the results of the paper together with the details of the MC simulation provided in the previous section of the supplement, we invite the experimental collaborations to perform their own dedicated analysis of the reflected dark matter signal.

Given a total energy deposition $E_{\rm dep.} = E_\chi - E'_\chi$ from DM scattering on an atomic electron, the average number of produced quanta at the interaction point is,

$$\langle N_Q\rangle = \frac{E_{\rm dep.}}{W} = E_{\rm dep.} L_y + E_{\rm dep.} Q_y = \langle n_\gamma\rangle + \langle n_e\rangle, \tag{S12}$$

with $W = 13.7\,\text{eV}$ [S8, S9]. The quanta are partitioned into n_e ionized electrons escaping the interaction point and n_γ scintillation photons; Q_y and L_y denote the energy-dependent charge and light yields, respectively. For the purpose of setting limits we only use data above $E_{\rm dep.} = 0.19\,\text{keV}$ in the computation of $\langle n_e\rangle$, corresponding to the lowest energy at which Q_y was measured [S10].[1] In addition, data on Q_y from [S12] is used; see also [S13, S14]. The light output is then obtained self-consistently by demanding conservation of N_Q,

$$L_y = \frac{1}{W} - Q_y. \tag{S13}$$

For $E_{\rm dep.} \lesssim 10$ keV the charge and scintillation yields depend only mildly on the applied drift voltage [S13, S15, S16]; for given $E_{\rm dep.}$, Q_y (L_y) varies by about 10% in the range $120 - 730$ V/cm, *i.e.* in the range of applied drift-fields accross the various experiments. We hence neglect this experiment-specific detail as it is expected to have only relatively minor impact on the resulting bounds. Finally, heat losses lead to a quenching in the nuclear recoil signal, and subsequently to a fluctuation in N_Q. For electron recoils, heat losses are negligible [S13, S15] and we take the number of produced quanta for a given deposited energy as a constant, $N_Q = \langle N_Q\rangle$.

Fluctuations at the interaction point

Recombination at the interaction point shifts the partition of n_γ and n_e while holding their sum $N_Q = n_\gamma + n_e$ fixed. The quantities n_γ and n_e are the end products after an initial number of ions n_i (yielding electrons) and excitons n_{ex} (yielding scintillation) had been created but were redistributed because of recombination described by parameter r, $n_e = n_i(1-r)$, $n_\gamma = n_i(r+\alpha)$, with $\alpha \equiv n_{ex}/n_i$. Note that $N_Q = n_\gamma + n_e = n_i + n_{ex}$. Fluctuations in r itself, leading to an observed variance that is in excess from one that is expected from a binomial process, are most important for larger energy depositions $E_R \gtrsim 2\,\text{keV}$ [S9, S12]; see also [S16]. Since the bulk of the solar flux is energetically lower, we neglect this complication. Thus, we follow [S6] and approximate the primary signal formation by directly computing the probabilities of producing either n_γ or n_e as,

$$P(n_{e,\gamma}|\langle n_{e,\gamma}\rangle) = \text{binom}(n_{e,\gamma}|N_Q, f_{e,\gamma}) \tag{S14}$$

where, $f_{e,\gamma} = n_{e,\gamma}/N_Q$, such that $f_e + f_\gamma = 1$. Since $\sigma^2_{e,\gamma} = f_{e,\gamma}(1-f_{e,\gamma})N_Q$ it follows that $\sigma^2_\gamma = \sigma^2_e$ and $P(n_e|\langle n_e\rangle) = P(n_\gamma|\langle n_\gamma\rangle)$.

Detector-specific fluctuations

The S1 signal is obtained from the probability of detecting $n_{\rm PE}$ photons from n_γ produced, and is modelled by a binomial distribution with overall light collection efficiency g_1 (the experiment-specific values of g_1 are found in the main text),

$$P(n_{\rm PE}|n_\gamma) = \text{binom}(n_{\rm PE}|n_\gamma, g_1). \tag{S15}$$

---

[1] After initial submission of the manuscript, a preprint of the measurement became available on arXiv [S11].

For computing the S2 signal, one needs to account for the survival probability $p_{\rm surv}$ of electrons when they are drifted by a distance Δz until the liquid-gas interface with a ballpark velocity $v_d \sim 1.7{\rm mm}/\mu{\rm s}$ [S5, S17],

$$p_{\rm surv} = \exp\left(-\frac{\Delta z}{\tau v_d}\right). \tag{S16}$$

The electron lifetime varies across experiments. We follow the reasoning presented in [S6] and assume that the electron lifetime is distributed uniformly over $[0, 2/3]$ mm/μs. The probability of $n_e^{\rm surv}$ electrons reaching the gas-phase of the detector is then found from the compound distribution function, where one marginalizes over the production location,

$$P(n_e^{\rm surv}|n_e) = \frac{3}{2}\int_0^{2/3} d\left(\frac{\Delta z}{\tau}\right)\, {\rm binom}(n_e|p_{\rm surv}(\Delta z/\tau)). \tag{S17}$$

To relax the numerical demand, in the actual analysis we assign an average electron survival probability $P(n_e^{\rm surv}|n_e) \simeq \langle p_{\rm surv}\rangle = 0.8$ obtained from the expectation value of (S16) which then allows to perform the sum in (S22) below.

In a final step we account for the PMT resolution, using as a representative value $\sigma_{\rm PMT} \simeq 0.4\sqrt{n_{\rm PE}}$ for the low-photon count in S1. For S2, once the electron reaches the gas phase it receives a gain factor g_2 in the number of produced photo-electrons that are detected (for the experiment-specific values of g_2 see main text). The process is modeled by a Gaussian with representative standard deviation $\sigma_{S2} = 7\sqrt{n_e^{\rm surv}}$ [S18]. The respective probabilities of detection read,

$$P(S1|n_{\rm PE}) = {\rm gauss}(S1|n_{\rm PE}, \sigma_{\rm PMT}), \tag{S18}$$

$$P(S2|n_e^{\rm surv}) = {\rm gauss}(S2|g_2 n_{e^{\rm surv}}, \sigma_{S2}). \tag{S19}$$

Collecting all factors allows one to estimate the correlated PDF for observing S1 and S2, given an energy deposition of $E_{\rm dep.}$,

$$P(S1, S2|E_R) = \sum_{n_e^{\rm surv}}\sum_{n_{\rm PE}}\sum_{n_\gamma} P(S2|n_e^{\rm surv})P(S1|n_{\rm PE})P(n_e^{\rm surv}|n_e)P(n_{\rm PE}|n_\gamma)P(n_\gamma|\langle n_\gamma\rangle). \tag{S20}$$

Such expression for the joint PDF in S1 and S2 makes it amenable to a likelihood analysis of the experimental data. For the purpose of this paper, where we primarily explore the principal experimental sensitivity and do not intend to forestall a dedicated experimental analysis, we consider the signals S1 and S2 separately, leaving an analysis in the correlated signal for more in-depth work. The pdf for S1 is then obtained from,

$$P(S1|E_R) = \sum_{n_{\rm PE}}\sum_{n_\gamma} P(S1|n_{\rm PE})P(n_{\rm PE}|n_\gamma)P(n_\gamma|\langle n_\gamma\rangle) = \sum_{n_{\rm PE}} P(S1|n_{\rm PE})\,{\rm binom}(n_{\rm PE}|N_Q, f_{\rm PE}f_\gamma), \tag{S21}$$

where in the last equality we have performed the sum over n_γ. For obtaining the PDF in S2 only, one evaluates,

$$P(S2|E_R) = \sum_{n_e^{\rm surv}}\sum_{n_e} P(S2|n_e^{\rm surv})P(n_e^{\rm surv}|n_e)P(n_e|\langle n_e\rangle). \tag{S22}$$

Of course, the PDFs (S21) and (S22) also follow directly from (S20) by marginalizing over S2 and S1, respectively.

DETAILS ON THE EXEMPLARY DM MODEL

The nonrelativistic scattering cross section on free electrons obtained from the Lagrangian given in the main text is found to be

$$\sigma_e = \frac{1}{\pi}G_{\chi e}^2\mu^2, \tag{S23}$$

where μ is the reduced mass. In turn, the total annihliation cross section to electrons in terms of the squared center-of-mass energy s reads,

$$\sigma_{\rm ann}(s) = \frac{G_{\chi e}^2}{12\pi s}(s+2m_e^2)\sqrt{s-4m_\chi^2}\sqrt{s-4m_e^2} \tag{S24}$$

In the non-relativistic expansion, $s = 4m_\chi^2 + m_\chi^2 v$, and one finds the velocity scaling corresponding to p-wave annihilation,

$$\sigma_{\rm ann} v = v^2 \times \frac{G_{\chi e}^2}{12\pi}(m_e^2 + 2m_\chi^2)\sqrt{1 - \frac{m_e^2}{m_\chi^2}}. \tag{S25}$$

We have calculated the relic abundance with three different methods: semi-analytically following [S19], numerically following [S20], and through an implementation of the publicly available computer code Micromegas [S21] with mutually agreeing results. Imposing the relic density condition, allows one to obtain the expectation for σ_e as a function of m_χ as provided in the main text. Within this model, the area below the line is disfavored by DM overproduction, while the area above the line makes χ to form only a fraction of the total DM energy density.

[S1] J. N. Bahcall, A. M. Serenelli, and S. Basu, Astrophys. J. **621**, L85 (2005), arXiv:astro-ph/0412440 [astro-ph].
[S2] A. Serenelli, S. Basu, J. W. Ferguson, and M. Asplund, Astrophys. J. **705**, L123 (2009), arXiv:0909.2668 [astro-ph.SR].
[S3] R. Essig, J. Mardon, and T. Volansky, Phys. Rev. **D85**, 076007 (2012), arXiv:1108.5383 [hep-ph].
[S4] B. M. Roberts, V. A. Dzuba, V. V. Flambaum, M. Pospelov, and Y. V. Stadnik, Phys. Rev. **D93**, 115037 (2016), arXiv:1604.04559 [hep-ph].
[S5] E. Aprile *et al.* (XENON100), Astropart. Phys. **54**, 11 (2014), arXiv:1207.3458 [astro-ph.IM].
[S6] R. F. Lang, C. McCabe, S. Reichard, M. Selvi, and I. Tamborra, Phys. Rev. **D94**, 103009 (2016), arXiv:1606.09243 [astro-ph.HE].
[S7] C. McCabe, (2017), arXiv:1702.04730 [hep-ph].
[S8] C. E. Dahl, *The physics of background discrimination in liquid xenon, and first results from Xenon10 in the hunt for WIMP dark matter*, Ph.D. thesis, Princeton U. (2009).
[S9] D. S. Akerib *et al.* (LUX), Phys. Rev. **D95**, 012008 (2017), arXiv:1610.02076 [physics.ins-det].
[S10] D. Huang, Ultra-low Energy Calibration of LUX Detector using D-D Neutron, Tritium and 127Xe, UCLA DM 2016.
[S11] D. S. Akerib *et al.* (LUX), (2017), arXiv:1709.00800 [physics.ins-det].
[S12] D. S. Akerib *et al.* (LUX), Phys. Rev. **D93**, 072009 (2016), arXiv:1512.03133 [physics.ins-det].
[S13] M. Szydagis, A. Fyhrie, D. Thorngren, and M. Tripathi, *Proceedings, LIght Detection In Noble Elements (LIDINE2013): Batavia, USA, May 29-31, 2013*, JINST **8**, C10003 (2013), arXiv:1307.6601 [physics.ins-det].
[S14] L. W. Goetzke, E. Aprile, M. Anthony, G. Plante, and M. Weber, (2016), arXiv:1611.10322 [astro-ph.IM].
[S15] M. Szydagis, N. Barry, K. Kazkaz, J. Mock, D. Stolp, M. Sweany, M. Tripathi, S. Uvarov, N. Walsh, and M. Woods, JINST **6**, P10002 (2011), arXiv:1106.1613 [physics.ins-det].
[S16] B. Lenardo, K. Kazkaz, A. Manalaysay, J. Mock, M. Szydagis, and M. Tripathi, IEEE Trans. Nucl. Sci. **62**, 3387 (2015), arXiv:1412.4417 [astro-ph.IM].
[S17] J. Yoo and W. F. Jaskierny, JINST **10**, P08011 (2015), arXiv:1508.05903 [physics.ins-det].
[S18] E. Aprile *et al.* (XENON100), J. Phys. **G41**, 035201 (2014), arXiv:1311.1088 [physics.ins-det].
[S19] K. Griest and D. Seckel, Phys. Rev. **D43**, 3191 (1991).
[S20] P. Gondolo and G. Gelmini, Nucl. Phys. **B360**, 145 (1991).
[S21] G. Belanger, F. Boudjema, A. Pukhov, and A. Semenov, Comput. Phys. Commun. **176**, 367 (2007), arXiv:hep-ph/0607059 [hep-ph].